NUMERICAL SIMULATION OF TEMPERATURE DISTRIBUTION AND MATERIAL FLOW DURING FRICTION STIR WELDING OF MAGNESIUM ALLOY

Evgenii N. Rylkov[1], Anton A. Naumov[1], Fedor Yu. Isupov[1], Oleg V. Panchenko[1], Anatoliy A. Popovich[1]

[1]National Technology Initiative Center of Excellence in Advanced Manufacturing Technologies at Peter the Great St. Petersburg Polytechnic University, St. Petersburg, Russia

Keywords: Friction stir welding; CFD simulation; Temperature field; Material flow; Mg alloy

Abstract

Magnesium alloys are widely used in aerospace industries and are very prospective to use in automotive industry, but the joining of Mg-based alloys by means of fusion welding techniques causes a number of difficulties. The solid-state joining techniques, such as friction stir welding (FSW), can be successfully used to join this type of alloys.

In the present research parameters of FSW are selected to produce defect-free joints, the CFD modeling was used to describe the temperature field and material flow during FSW of magnesium alloy. Developed model was used to determine the temperature field and material flow around the tool.

Introduction

Today, many industries, such as automotive, aerospace, shipbuilding and many others are engaged in the challenge of structures weight reduction to save the fuel or energy. For these reasons, magnesium alloys are used as engine chassis, wheel rims, mobile cranes and frames, fuel tanks, wings, masts, booms etc. But the joining of Mg-based alloys by fusion welding techniques causes a number of difficulties, thus industries have to use the joining techniques, such as friction stir welding (FSW).

It is well-known, that FSW is a complex thermo-mechanical process. The complexity of material flow during FSW is a result of severe plastic deformation realized at high strain rates [1-3]. During welding, heat generates from friction contact between the tool and work-pieces and there are different approaches to simulate the process. This work was used as a Eulerian approach that utilizes the Computational Fluid Dynamics (CFD) technique. In this approach material is presented as high viscous liquid flow. The first works in this direction were made by Colegrove and Shercliff [4-7]. They aimed to analyze the flow patterns, the influence of tool, temperature field. Later many authors used that approach, Hassan and Bennet used it to predict the tool wear [8]; Suresh and Mandhusudnal - to effect of tool tilt angle [9]; Sun and Wu - to modeled probe thread effect [10]; Behzad and Aboozar - to predict weld morphology in dissimilar joints [11]. All these works show that CFD approach gives reliable results.

In this current study, the CFD model was developed, different regimes of FSW process were simulated before welding. Based on simulation result one regime of FSW process was selected and realized.

Experimental Procedure

Model description

In this work was used commercial CFD software FLUENT. Four different FSW regimes ware simulated (Table I). Initial source data for simulation were material properties, tool rotation speed, and welding speed. Output data were the next: an axial force, temperature distribution and material flow.

The optimal regime was selected by analyzing temperature distribution near the tool. On the assumption that elevated temperatures, but lower than melting point, provide lower viscosity and better mixing of the material, one regime was selected.

Table I. FSW regimes

Number	1	2	3	4
Rotation speed, RPM	500	1000	2000	3000
Welding speed, mm/min	300	300	300	300
Heat Input (Rot. speed / Weld. speed)	~1,66	~3,33	~6,66	10

To predict the axial force, it is necessary to set tool angle. In all cases the tool angle was 2 degrees.

The computational domain of the FSW models, tool position and tool geometry are showed in Fig. 1. Domain represents sheet with dimensions of 2 mm high, 200 mm length, 150 mm wide with tool ‘imprint’. It should be noted that the tool is in contact with the workpiece only by part of the shoulders surface (Fig. 1 b).

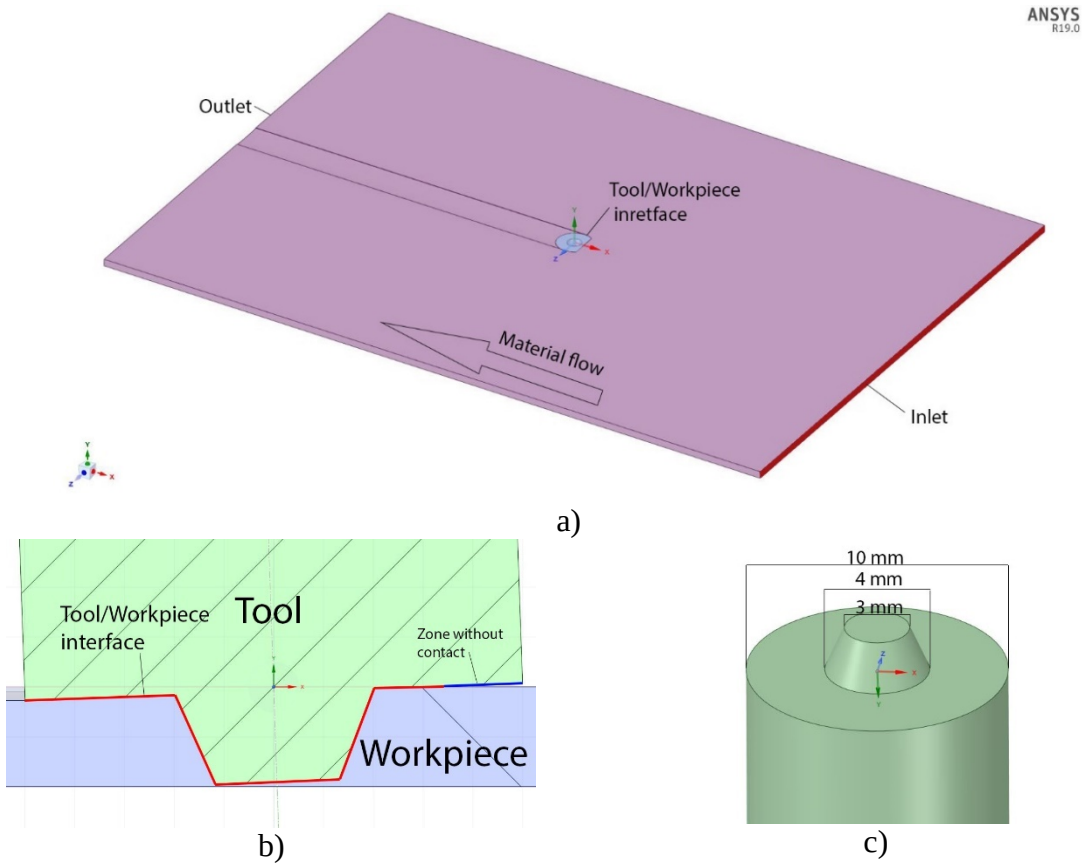

Figure 1. Scheme of the domain (a), tool position (b), tool geometry (c)

Material flows into the computational domain through the 'Inlet' and 'Outlet' boundaries with 300 mm/min speed which is equal to the welding speed in the experiment. The speeds of the 'Sides', 'Top surface' and 'Down surface' are also set as 300 mm/min. The contact heat transfer coefficient of the 'Down surface' is 800 W/m^{2}K, at another surface 30 W/m^{2}K. The surface that contact with tool is rotating around the Y axis with the speed according to the regime. This CFD model contains 8637083 tetrahedral cells.

Based on works [12-15], a frictional boundary condition is applied in this study. The frictional stress at the interface is calculated by the equation (1) [9].

$$\vec{\tau}_f = \begin{cases} \mu_f \sigma_n \frac{\vec{\upsilon}_{vel}}{\vec{\upsilon}_{vel}} \tanh(\alpha \vec{\upsilon}_{vel}), if\ \vec{\upsilon}_{vel} \neq 0 \\ 0, if\ \vec{\upsilon}_{vel} = 0 \end{cases} \quad (1)$$

Where $\vec{\upsilon}_{vel}$ is the relative velocity between the tool and material; α = 20 s/m is a scaling constant; μ_f is the sliding friction coefficient; σ_n is the normal pressure at the welding tool/workpiece interface. It should be noted that in this work normal pressure is calculated at each cell face at tool/workpiece interface, that provide ability to calculate axial force. The friction coefficient is defined as 0.4 and after temperature equals to 550 C° (solidus temperature minus 50 C°) linearly decreases to 0 at solidus temperature, as shown in Fig. 2 a. The estimated solidus temperature of this material is 598 C°.

Frictional heat and plastic deformation heat are considered in this CFD model, the interfacial friction heat is given as follows [9].

$$q_f = \eta \left\| \vec{\tau}_f \right\| \left\| \vec{\upsilon}_{vel} \right\| \quad (2)$$

Where $\vec{\tau}_f$ is the frictional tangential force; $\vec{\upsilon}_{vel}$ is the relative velocity between the welding tool and the workpiece; η is the ratio of the heat absorbed by the workpiece and is used as 0.7 [16]. Plastic deformation heat will be generated in the deformation zone, which is too high to be ignored. The plastic deformation heat is given by equation (3):

$$q_p = K\sigma\dot{\varepsilon} \quad (3)$$

Where K = 0.6 is the mechanical efficiency; σ is the flow stress, $\dot{\varepsilon}$ is the effective strain rate.

Materials

In this work MgAl2Zn alloy was used, the chemical composition is shown in Table II. Flow stress of the workpiece is considered to be temperature and strain rate dependent and can be obtained through empirical equation (4) [14].

$$\sigma_F = A e^{m_1 T} \varepsilon^{m_2} e^{m_4/\varepsilon} (1+\varepsilon)^{m_5 T} e^{m_7 \varepsilon \dot{\varepsilon}^{\cdot m_8 T}} \quad (4)$$

Where σ_F is flow stress, ε is a strain, A is a constant, m1 to m8 are exponents expressing the influence of the deformation conditions on the stress and T is the deformation temperature in C°. In this work ε is a constant equal to 1.2, as a maximum value in the range of validity [17] $\dot{\varepsilon}$ is an effective strain rate, which is determined by the equation (5).

$$\dot{\varepsilon} = \sqrt{\frac{2}{3} \dot{\varepsilon}_{ij} \dot{\varepsilon}_{ij}} \quad (5)$$

Where $\dot{\varepsilon}_{ij}$ is the component of strain rate tensor, which is determined by the equation (6).

$$\dot{\varepsilon}_{ij} = \frac{1}{2}\left(\frac{dv_i}{dx_j} + \frac{dv_j}{dx_i}\right) \quad (6)$$

Because there is an error between the calculated results and the experimental data at a temperature close to solidus the flow stress at high temperature is modified by the method used in the literature [7]. The viscosity of the material during the simulation of FSW can be determined by the equation (7) [4-7].

$$\mu = \frac{\sigma}{3\dot{\varepsilon}} \quad (7)$$

The heat capacity and thermal conductivity of the workpiece are temperature dependent, as shown in Fig. 2 b.

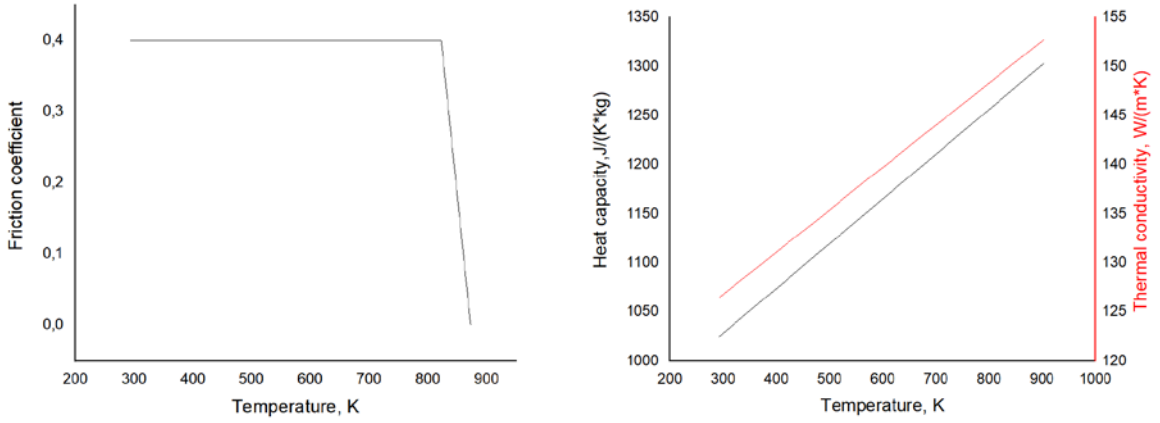

Figure 2. Friction coefficient temperature dependence (a), heat capacity and thermal conductivity temperature dependence (b)

Table II. Chemical composition MgAl2Zn alloy

Mg	Al	Mn	Fe	Si	Ni	Other elements
Bal.	<0.010	<0.004	<0.003	<0.005	<0.001	<0.005

Results and Discussion

Fig 3 shows the temperature field near the tool at different regimes. Table III shows calculated axial force at different regimes. Total force was computed as a sum of forces along Y-axis of each face of a cell at tool/workpiece interface. Fig. 4 shows the isosurface at temperature equals to 550 C° at different regimes. The isosurface of regime №1 was not plotted, because there were no cells with a temperature above solidus.

From the results it can be seen that temperature distribution is asymmetric, higher temperatures are at retreating side closer to the back of the tool. At regimes №1 and №2 the temperature distribution is less homogeneous, at retreating side the zone with high temperature was formed. Also, at these regimes temperature at the center of the probe bottom is about 418-450 C°, which may not be enough to plasticize the material. Presumably, the defects may be formed at these regimes. In Fig. 4 d it can be seen that at regime №4 isosurface bigger than tool ‘imprint’, in this case, the flashes may be formed.

Analyzed temperature field for regime №3 was selected for real experiments. This regime was realized at the FSW machine with force control. The obtained joint is showed in Fig. 5.

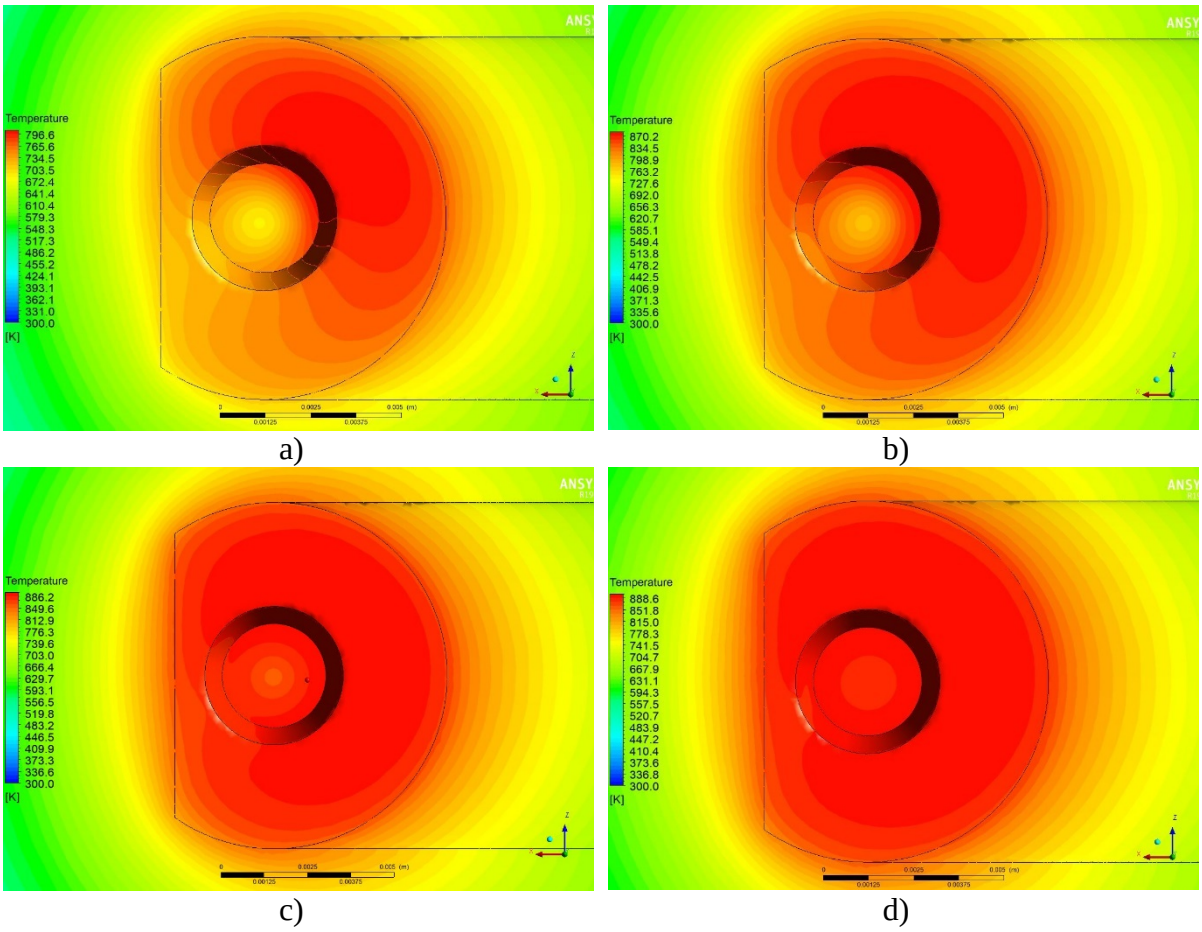

Figure 3. Temperature field near the tool (a) regime №1, (b) regime №2, (c) regime №3, (d) regime №4

Table III. Calculated axial force

Regime number	1	2	3	4
Axial force, N	3988.23	2642.53	1702.96	972.383

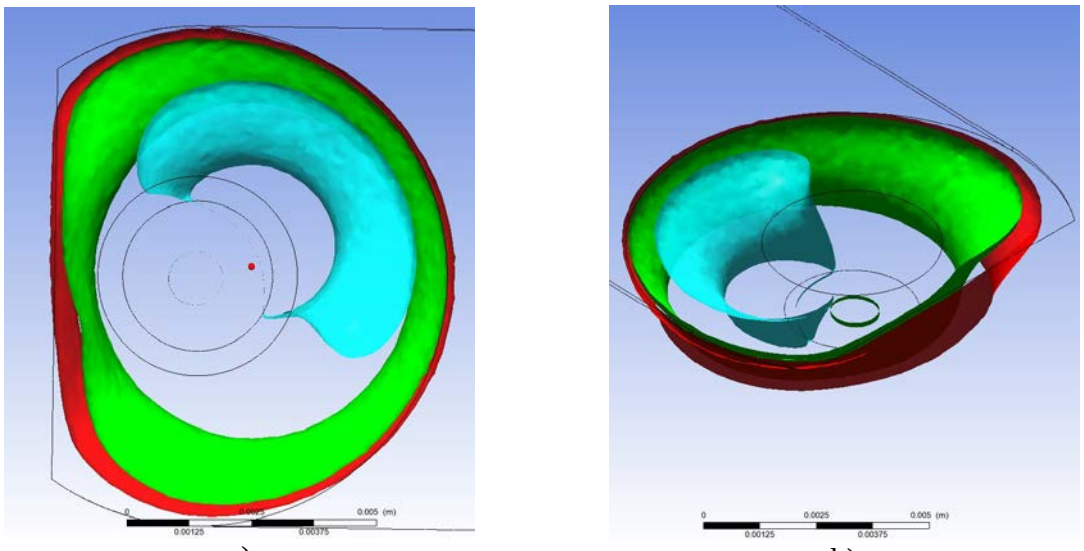

Figure 4. Temperature isosurface, red – regime №4, green – regime №3, blue regime №2, (a) top view, (b) isometry.

Figure 5. Joint obtained by regime №3.

Conclusion

1. The results of simulating are reliable. Analysis of the temperature distribution near the tool can predict the quality of the weld. Hight temperature, but lower than solidus, provide defect-free joint.
2. The model is able to predict axial force. Based on the simulation results one regime (№3) was selected and realized on FSW machine. The obtained joint is visual defect-free.

Acknowledgments

This work is supported by the Russian Science Foundation under grant № 19-79-30002.

The results of the work were obtained using computational resources of Peter the Great Saint-Petersburg Polytechnic University Supercomputing Center (www.spbstu.ru).

References

1. A.I. Rudskoy et al., "Advanced metallic materials and processes," *Materials Physics and Mechanics*, 25 (1) (2016), 1-8.
2. R.A. Parshikov, et al., "Analysis of specimen plastic flow features during severe plastic deformation," *Reviews on Advanced Materials Science*, 45 (1-2) (2016), 67-75.
3. F. Grechnikov, A. Khaimovich, "The study of plastic deformation at high strain rates in upset forging of cylinders," *Key Engineering Materials*, 684 (7) (2016), 74-79.
4. P.A. Colegrove, H.R Shercliff, "Two-dimensional CFD modelling of flow round profiled FSW tooling," *Friction Stir Welding and Processing II*, (2003), 13-22.
5. P.A. Colegrove et al., "Development of Trivex friction stir welding tool Part 1 – two-dimensional flow modelling and experimental validation," *Science and Technology of Welding and Joining*, 9 (4) (2004), 345-351.
6. P.A. Colegrove et al., "3-Dimensional CFD modelling of flow round a threaded friction stir welding tool profile," *Journal of Materials Processing Technology*, 169 (2) (2005), 320-327.
7. P.A. Colegrove, "CFD modelling of friction stir welding of thick plate 7449 aluminium alloy," *Science and Technology of Welding and Joining*, 11 (4) (2005), 429-441.
8. A.F. Hasan et al., "A numerical comparison of the flow behaviour in Friction Stir Welding (FSW) using unworn and worn tool geometries," *Materials and Design*, 87 (15) (2015), 1037-1046.
9. M.D. Suresh et al., "Influence of Tool Tilt Angle on Material Flow and Defect Generation in Friction Stir Welding of AA2219," *Defence Science Journal*, 68 (5) (2018), 512-518.

10. Z. Sun et al., “A numerical model of pin thread effect on material flow and heat generation in shear layer during friction stir welding, ” *Journal of Manufacturing Processes,* 36 (S) (2018), 10-21.
11. B. Sadeghian et al., “Simulation of weld morphology during friction stir welding of aluminum- stainless steel joint, ” Journal of Materials Processing Technology, 259 (F) (2018), 96-108.
12. G. Chen et al., “An alternative frictional boundary condition for computational fluid dynamics simulation of friction stir welding,” *Journal of Materials Engineering and Performance,* 25 (9) (2016), 4016–4023.
13. Zhu Y et al., “Simulation of material plastic flow driven by nonuniform friction force during friction stir welding and related defect prediction,” *Materials and Design,*108 (15) (2016), 400–410.
14. Chen G et al., “Effects of pin thread on the in-process material flow behavior during friction stir welding: a computational fluid dynamics study, ” *Int J Mach Tools Manuf,* 124 (J) (2018), 12-21.
15. S. Zhang et al., “Numerical analysis and analytical modeling of the spatial distribution of heat flux during friction stir welding,” *Journal of Manufacturing Processes,* 33 (2018), 245-255.
16. A. Bastier et al., “Steady state thermomechanical modelling of friction stir welding,” *Sci Technol Weld Join,* 11 (3)(2006), 278–288.
17. Marlene Spittel and Thilo Spittel, *Numerical Data and Functional Relationships in Science and Technology Group VIII: Advanced Materials and Technologies Metal Forming Data - Volume 2: Materials Part 2: Non-ferrous Alloys - Light Metals,* (Berlin, Springer-Verlag Berlin Heidelberg 2016), 26.